ACS OMEGA

http://pubs.acs.org/journal/acsodf

Article

F^- Serve as Surface Trapping Sites to Promote the Charge Separation and Transfer of TiO_2

Xiaogang Liu,* Wenjie Chen, and Wei Wang

Cite This: *ACS Omega* 2021, 6, 35799−35809

Read Online

ACCESS | Metrics & More | Article Recommendations | Supporting Information

ABSTRACT: Finding an effective strategy to promote the charge transfer and separation of TiO_2 is urgently needed. Herein, a surface fluorination (F^-)-modified TiO_2 (denoted as TO-*x*F, where *x* represents the volume of HF added in the solution) catalyst has been prepared by a mild and facile post-treatment method. The changes induced by surface F^- on the morphological, structural, and surface electronic features and the charge separation and transfer efficiency of TiO_2 were specifically examined. Compared with pristine TO, TO-0.4F exhibits enhanced photocatalytic degradation of methyl orange and phenol, production of hydroxyl radicals, and photocurrent response. The enhanced photocatalytic activities of TO-0.4F can be attributed to the role of surface F^- as surface trapping sites in effectively boosting the charge transfer and separation processes, which is verified by the steady-state and time-resolved fluorescence spectroscopy, electrochemical impedance spectroscopy, Bode plot, transient photocurrent response, and open-circuit voltage measurements. This study emphasizes the role of surface F^- in promoting the charge transfer and separation and improving the photocatalytic activity of TiO_2.

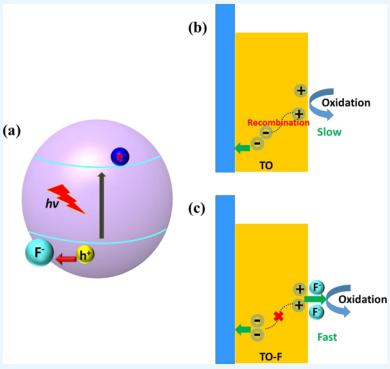

1. INTRODUCTION

As a typical semiconductor, titanium dioxide (TiO_2) has received extensive attention due to its high stability, nontoxicity, facile and low-cost synthesis, and tunable electronic band structure features. Particularly, TiO_2-based semiconductor materials have been extensively used in a wide range of applications, such as H_2 production,[1−3] CO_2 reduction,[4−7] nitrogen fixation,[8−10] wastewater treatment,[11−13] gas sensors,[14,15] and solar cells.[16,17] However, the ineffective separation and transport of charge carriers as a consequence of a shorter carrier lifetime largely restricts its application of photogenerated carriers for photoelectrochemical and chemical reactions.[18−20] Thus, research studies were tremendously intensified to overcome these bottlenecks, and momentous advancements were attained over the past few decades. Generally, strategies proposed to boost the separation and transport efficiency of charge carriers were developed, such as morphology modulation,[21−23] crystal facet engineering,[24−26] element doping,[27−30] heterostructure construction,[18,31−34] cocatalyst loading,[35,36] plasma enhancement,[37,38] and combinations thereof.[39] Though these approaches were devoted to facilitate charge transfer to a certain degree, the vast majority of photoinduced electrons and holes still recombined during the charge transportation process, and the photocatalytic performance of TiO_2 was still far from satisfactory. Hence, it is of great significance to develop highly efficient TiO_2.

Recent research results show that the post-treatment procedure after sample preparation has emerged as an attractive strategy to effectively address the issue of separation and transport of charge carriers over semiconductor photocatalysts.[40,41] For example, a facile and efficient Cl^- surface modification method has been demonstrated earlier to drastically enhance photocatalytic water oxidation over a $BiVO_4$ catalyst.[40] Due to the acceleration of photogenerated holes by Cl^-, as-prepared Cl^--modified $BiVO_4$ achieved excellent oxygen evolution, whose apparent quantum efficiency could reach 34.6% at 420 nm. Moreover, Cl^--modified Bi_2WO_6 nanosheets were prepared to examine their photocatalytic oxidation performance.[42] It is surprising to find that the CH_4 yield of Cl^--modified Bi_2WO_6 was almost 10 times of that obtained with the pristine Bi_2WO_6 one. These surface-modified catalysts with higher photoreactivity offer insights and provide more opportunity to promote the efficiency of separation and transport of carriers and enhance the photoreactivity of semiconductor photocatalysts.

Compared with Cl^-, fluorine (F^-) possesses the strongest electronegativity of 3.98, and it readily reacts with metal elements and oxidizes them to their highest valence states. Moreover, F^- has been widely used as a morphology directing agent to stabilize the {001} facet of TiO_2 since its initial use by Yang et al.[24] The effectiveness of F^- in obtaining TiO_2 crystals with a dominant {001} facet by forming the Ti−F bond to

Received: October 20, 2021
Accepted: December 8, 2021
Published: December 16, 2021

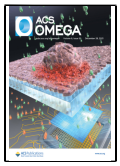

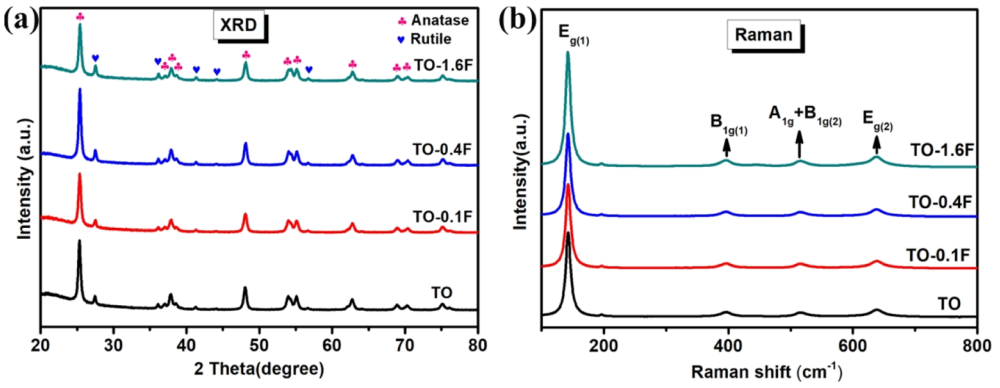

Figure 1. (a) XRD patterns and (b) Raman spectra of TO and TO-xF.

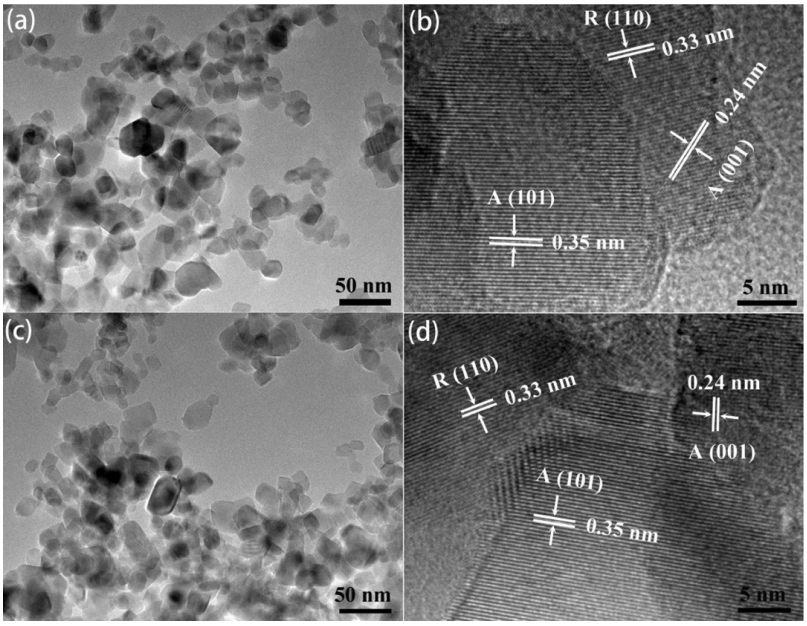

Figure 2. (a)TEM and (b) HRTEM images of TO. (c) TEM and (d) HRTEM images of TO-0.4F.

saturate surface Ti_{5c} has been confirmed by numerous studies.[25,43−45] Though fluorine can be partially removed by either washing with a basic solution or a calcination process, the role of residual F^- in influencing the electronic structure, charge transfer and separation behaviors and, ultimately, the photocatalytic activities of TiO_2 cannot be neglected. Moreover, fluorine can be introduced into TiO_2 to generate two forms of fluorine species: surface fluorine and lattice fluorine. The former is proved to influence the adsorption capacity, provide surface trapping sites, and regulate the charge transfer and storage.[46,47] The latter is commonly considered to form defective centers (Ti^{3+} or oxygen vacancy species) and introduce localized electronic states. F^- existing on the surface could affect the electronic structure of TiO_2 and exchange with the surface hydroxyl group (−OH). For instance, reported works showed that the displacement of the −OH group by F^- could regulate the kinetics and mechanism over the photocatalytic degradation of phenol.[48] Moreover, F^- may suffer from redox transformations after electron transfer with carriers and remarkably affect the photocatalytic activities depending on their affinity to the surface of the specified semiconductor. Consequently, the photoreactivity of surface F^--treated TiO_2 has been reported either to increase[49,50] or to decrease[51] compared with those of the pristine TiO_2 ones. Even so, evidence of the improved photocatalytic efficiency as well as its mechanism over surface-fluorinated TiO_2 is obscure and remain to be explored thoroughly, to obtain a high solar energy conversion and particularly a high-performance TiO_2 photocatalyst.

Herein, we report a facile F^- surface modification method, which not only improves the efficiency of charge separation but also accelerates the charge-transfer process. Compared with pristine TiO_2 (denoted as TO), F^- surface-modified TiO_2 (denoted as TO-*x*F, *x* represents the volume of HF added in the solution) of the TO-0.4F sample exhibits enhanced and optimal photocatalytic degradation of methyl orange (MO), photocatalytic production of the hydroxyl radical (HO•), and photocurrent response under UV light irradiation. Moreover, the improved charge carrier separation and transfer efficiency by surface F^- was verified by steady and time-resolved photoluminecence (PL) spectroscopy, electrochemical impedance spectroscopy (EIS), Bode plot, transient photocurrent response, and open-circuit voltage (U_{OC}) measurements.

https://doi.org/10.1021/acsomega.1c05891
ACS Omega 2021, 6, 35799−35809

2. MATERIALS AND METHODS

The detailed information of preparation, characterizations, photocatalytic generation experiment of •OH radicals, photocatalytic degradation of methyl orange (MO) and phenol, and photoelectrochemical measurements over as-prepared F^--modified TiO_2 can be found in the Supporting Information.

3. RESULTS AND DISCUSSION

The crystal structures of TO and TO-*x*F catalysts were determined by powder X-ray diffraction (XRD), as shown in Figure 1a. Both anatase and rutile phases are observed over pristine TO_2. More specifically, diffraction peaks at 2θ = 25.28, 36.95, 37.80, 38.58, 48.05, 53.89, 55.06, 62.69, 68.76, 70.31, 75.03, and 76.02° (JCPDS NO. 21-1272) are typically anatase TiO_2, while 2θ = 27.45, 36.09, 41.23, 44.05, and 56.64° (JCPDS NO. 21-1276) are peaks of rutile TiO_2. Moreover, it can be found that anatase is the dominant crystal phase in pristine TO. For TO-*x*F samples, peaks of anatase and rutile TiO_2 are also detected at the corresponding positions, while no other new diffraction peaks can be observed, which implies that F^- may have a negligible impact on the crystal structure of TiO_2. Besides, no diffraction peak shift is observed in TO-*x*F, suggesting the maintained crystal structure during the F^- post-treatment process. Figure 1b shows that all the TO and TO-*x*F catalysts exhibit typical Raman peaks at 143, 396, 516, and 638 cm^{-1}, which are assigned to $E_{g(1)}$, $B_{1g(1)}$, A_{1g} + $B_{1g(2)}$, and $E_{g(2)}$ vibration bands of anatase TiO_2, respectively. No signals of rutile TiO_2 could be observed, which can be explained by the relatively lower contents of rutile TiO_2 which were concealed by the strong Raman signals of anatase TiO_2.

The surface morphology and microstructures of as-prepared samples were observed by scanning electron microscopy (SEM) and transmission electron microscopy (TEM) analyses. As shown in Figure S1a, the TO sample displays an irregular morphology of nanoparticles, and the average particle size was about 20−25 nm. Moreover, the surface F^- modification has a negligible influence on the morphology and particle size, as shown in Figure S1b−d. Furthermore, TEM images analysis further confirms that the TO catalyst consists of irregular nanoparticles with an average particle size of 25 nm, as shown in Figure 2a. It can be seen from Figure 2b that pristine TO exhibits three obvious lattice fringes with spacings of 0.35, 0.24, and 0.33 nm, which corresponds to the (101) and (001) facets of anatase TiO_2 and (110) facet of rutile TiO_2, respectively. After F^- surface modification, the micromorphology of TO-0.4F in Figure 2c has no obvious changes compared with pristine TO. Similarly, the lattice fringes of both anatase and rutile TiO_2 appear in Figure 2d. Moreover, no lattice fringes of bulk fluoride species can be observed, which indicates that HF post-treatment does not result in the bulk fluorination of the TO catalyst in our present work. To further verify the components of the F^--treated TO sample, the energy-dispersive X-ray (EDX) elemental mapping images of the TO-0.4F catalyst are provided. As can be seen from Figure 3a−d, Ti, O, and F elements are homogeneously distributed in the TO-0.4F catalyst. In addition, the EDX patterns of as-prepared TO-0.4F are also performed, as shown in Figure S2.

The effect of F^- toward the surface element compositions and states over the prepared catalysts is examined by XPS characterization. As depicted in Figure 4a, the TO catalyst exhibits two typical XPS peaks located at 458.39 (Ti $2p_{3/2}$) eV and 464.11 eV (Ti $2p_{1/2}$), indicating the existing Ti^{4+} state in

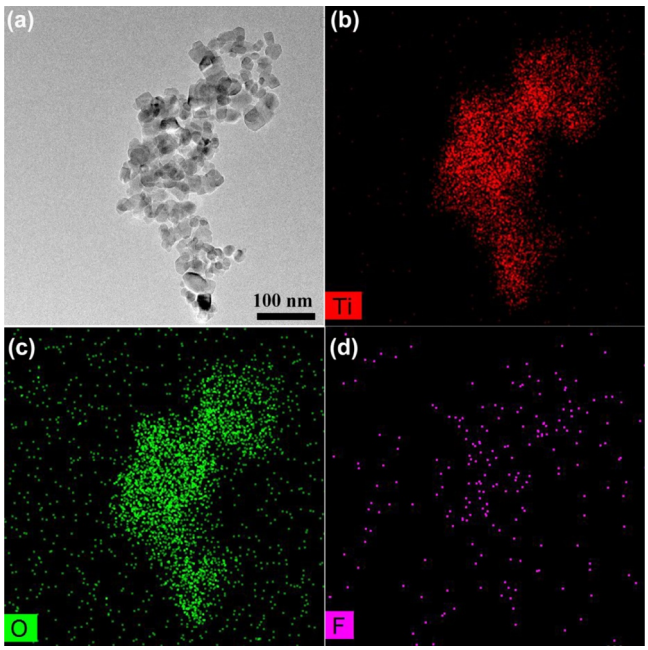

Figure 3. TEM image (a)and EDX mapping of Ti (b), O (c), and F (d) elemental distribution over TO-0.4F.

the crystal structure of TiO_2.[34] Notably, the characteristic Ti^{4+} peaks shift to a higher and then lower binding energy positions after F^- modification on the surface of TiO_2. More specifically, the Ti $2p_{3/2}$ position of TO-0.1F, TO-0.4F, and TO-1.6F catalysts shifts to 458.48, 458.56, and 458.22 eV, respectively. This obvious shift may come from a charge imbalance induced by F^- modification on the surface of TiO_2.[52] Moreover, this suggests that the electron cloud density of Ti on the surface of TO-0.1F and TO-0.4F is slightly lower than that of Ti on the surface of pristine TO, which results from the electron transfer from Ti to F. However, too much F^- on the surface of TiO_2 is detrimental to the transfer of electron to F. The XPS results further confirm the existence of the electron interaction between F and Ti in the TO-xF catalysts. In addition, O 1s spectra of pure TO catalysts exhibit two XPS peaks at 531.51 and 529.63 eV, which are ascribed to the surface-adsorbed hydroxyl oxygen (O_{OH}) and lattice oxygen($O_{lattice}$), respectively. Similarly, the XPS peaks of O 1s (Figure 4b) for TO-0.1F and TO-0.4F also shift positively and then negatively for TO-1.6F, further indicating that F^- might have a vital influence on the surface chemical environment of TiO_2. Considering the crucial role of the hydroxyl group in influencing the catalytic performance of the TiO_2 catalyst, the proportion of the hydroxyl group in all oxygen atoms is estimated based on the corresponding XPS peak area, as summarized in Table S1. The percentage of hydroxyl oxygen atoms for TO is estimated to be 28.36%, while the value decreases to 21.26, 20.53, and 19.89% for TO-0.1F, TO-0.4F, and TO-1.6F, respectively. The reason for the decreased surface hydroxyl of TO-*x*F can be attributed the displacement of surface hydroxyl by F^- ions. It was reported that the displacement of surface −OH by F^- could change the adsorption and the surface interactions (e.g., the adsorption of oxygen followed by the production rate of superoxide would be strongly affected).[48,53] As shown in Figure 4c, compared with pure TO, TO-*x*F samples exhibit broad binding energy peaks centered ca. 684 eV, which are ascribed to the F species adsorbed on the TiO_2 surface.[24,54,55]

https://doi.org/10.1021/acsomega.1c05891
ACS Omega 2021, 6, 35799−35809

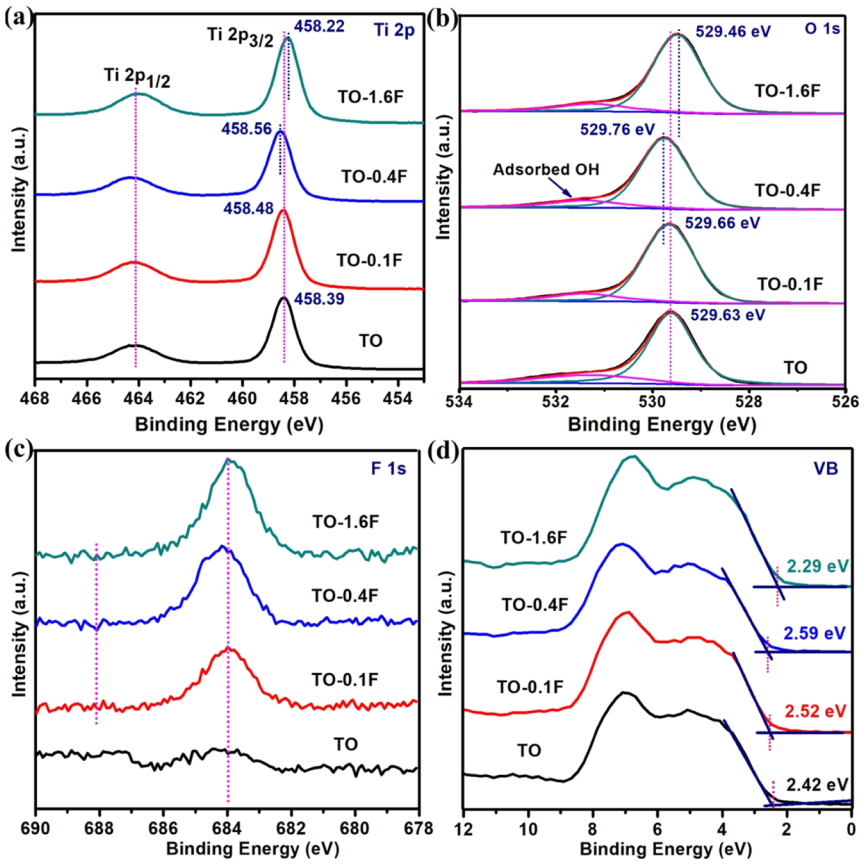

Figure 4. High-resolution XPS spectra of Ti 2p (a), O 1s (b), F 1s (c) and VB XPS spectra (d) for TO and TO-*x*F.

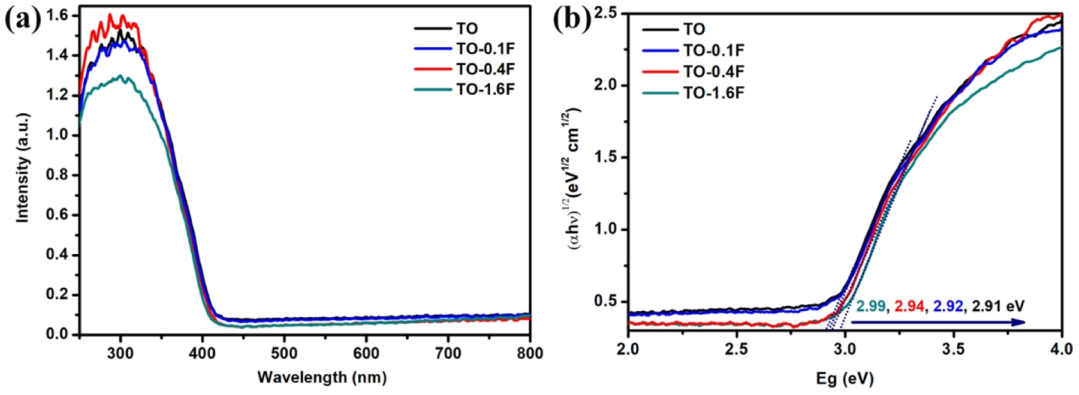

Figure 5. (a) Plot of UV−vis DRS and (b) Kubelka−Munk function plotted against the band gap energy for TiO_2.

Moreover, no lattice F or substituted F[27,56] (the corresponding XPS peaks usually centered at ca. 688 eV) of oxygen in the crystal surface of TiO_2 can be observed in the TO-xF catalyst. The band structure is very important for the photoreactivity because it largely influences the redox potential of the semiconductor photocatalyst. Therefore, the XPS valence band (VB) is examined, as shown in Figure 4d. The estimated VB positions of TO, TO-0.1F, TO-0.4F, and TO-1.6F are located at 2.42, 2.52, 2.59, and 2.29 eV, respectively. The shift of the VB energy level is possibly due to the F^- substitution of −OH on the surface of TiO_2.[47]

The optical absorbance properties of TO and TO-*x*F were examined. Figure 5a shows the UV−vis diffuse reflectance spectroscopy (DRS) spectra of TO, TO-0.1F, TO-0.4F, and TO-1.6F. TO-*x*F catalysts exhibit a slight shift of the absorbance toward the UV range compared with pristine TiO_2, which indicates the decreased utilization of the visible light region solar energy. The band gap energy (E_g) is estimated through an extrapolation method by fitting the linear part of the plot, as shown in Figure 5b. The calculated E_g are 2.99, 2.94, 2.92, and 2.91 eV for TO-1.6F, TO-0.4F, TO-0.1F, and TO, respectively.

Figure S3 displays the FTIR spectra of as-prepared TO and TO-xF catalysts. The region of the broad reflectance band at 3350 cm^{-1} for TO and TO-*x*F is generally ascribed to the characteristic band of the O−H stretching vibration related to the physical adsorbed water. Most importantly, compared with pure TO, the peak at 3350 cm^{-1}(O−H stretching) for TO-*x*F is markedly strengthened and, in particular, the peak intensities of TO-0.1F and TO-1.6F are stronger, indicating that surface-

https://doi.org/10.1021/acsomega.1c05891
ACS Omega 2021, 6, 35799−35809

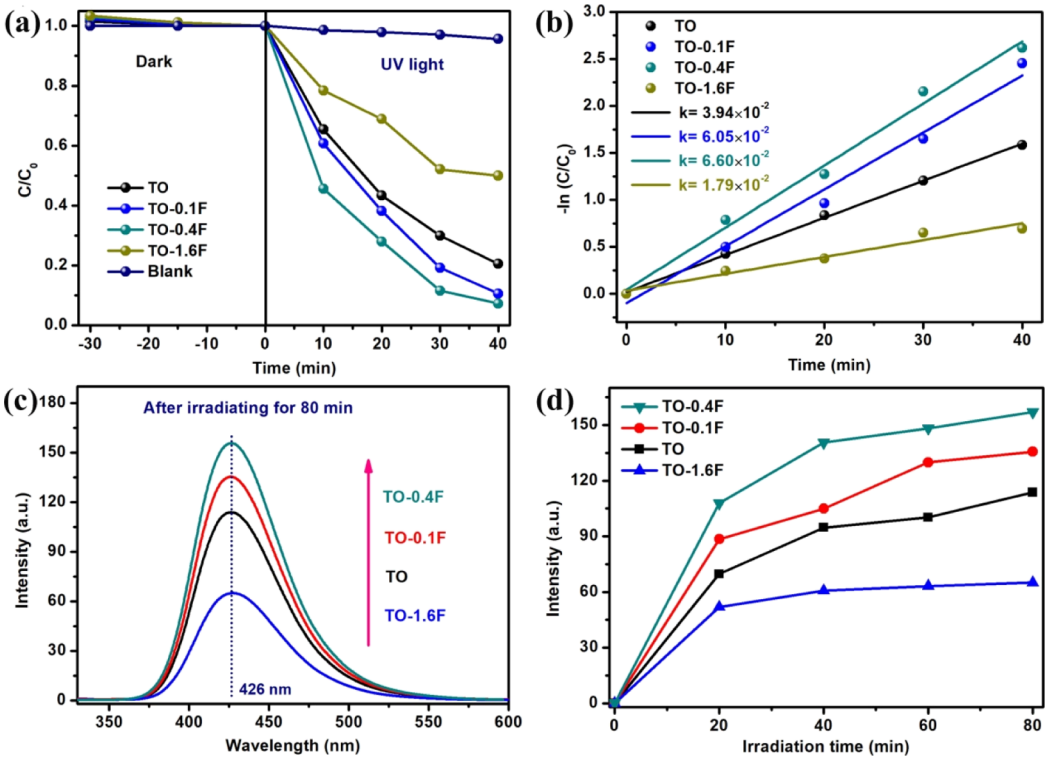

Figure 6. (a) Degradation performance of MO; (b) fitted curves of $-\ln(C/C0)$ vs reaction time; (c) comparison of •OH radicals recorded from fluorescence spectra; and (d) temporal profiles of •OH radicals over TO, TO-0.1F, TO-0.4F, and TO-1.6F.

modified F^- could affect the concentration of the surface-adsorbed OH groups. This can be further verified by the enhanced vibration peak at 1632 cm^{-1} for TO-0.1F, TO-0.4F, and TO-1.6F, which is an indicator of the O−H bending mode of water.[57] The FTIR results are well in accordance with our XPS result, further highlighting the role of F^- in affecting the surface OH groups of TiO_2. The adsorption of water by TiO_2 may be due to the presence of OH groups, or the stronger electron-acceptor centers, that is, the presence of coordinated unsaturated Ti^{4+} sites.[58] Additionally, the signals of the adsorbed CO_2 and related carbonate on the surface of TiO_2 at 2347, 1412, and 1339 cm^{-1}, which belong to an asymmetric stretching vibration of C−O, stretching and bending vibrations of C−OH and C−O bonds, respectively. Moreover, a sharp and strong peak centered near 673 cm^{-1} is observed for TO and TO-*x*F, which can be attributed to the Ti−O stretching band for the characteristic peaks of TiO_2 vibration.[59,60]

The specific surface areas and pore sizes of the as-prepared catalysts were determined from the nitrogen adsorption−desorption isotherms, as shown in Figure S4. All the TO and TO-*x*F samples show a typical IV adsorption−desorption isotherm with H2-type hysteresis loops, suggesting the presence of mesoporous structures. The specific surface areas calculated from the BET method are 54.00, 54.02, 50.86, and 55.24 $m^2 \cdot g^{-1}$ over TO, TO-0.1F, TO-0.4F, and TO-1.6F, respectively. In addition, by using the Barrett−Joyner−Halenda equation, the calculated average pore size is about 30 nm for TO and TO-*x*F samples. The specific surface area, pore volume, and average pore size of TO and as-prepared TO-*x*F catalysts are summarized in Table S2. Because the calculated porosity is equivalent to the size of the basic particles, it can be considered that the obtained mesopores come from substantial voids between the TiO_2 nanoparticles. Based on the above results, we confirm that surface F^- does not induce obvious textural changes of pristine TiO_2, which is well consistent with the SEM and TEM analyses.

The photocatalytic degradation of methyl orange (MO) under UV light is carried out, which is shown in Figure 6a. The pristine TO sample shows a high degradation efficiency of 79% toward MO after UV light irradiation for 40 min. In contrast, surface modification with a small amount of F^- on TO leads to an enhanced degradation efficiency of 89% for TO-0.1F. Furthermore, TO-0.4F shows the highest degradation efficiency of 95% among the F^--modified TiO_2 samples. However, the presence of too much F^- on the surface of TiO_2 brought about a noticeable decline of the photocatalytic degradation efficiency of 51% for the TO-1.6F catalyst. The activity of one catalyst is generally the result of interactions of various factors. In the current case, because the textural and morphological features of TiO_2 are almost retained before and after surface fluorination, the higher or lower photocatalytic efficiency of TO-*x*F can be related to the surface and optoelectronic features. The fitted curves of $-\ln(C/C_0)$ versus reaction time were plotted to determine the reaction rate constant (k), as shown in Figure 6b. Specifically, the k values are 3.94×10^{-2}, 6.05×10^{-2}, 6.60×10^{-2}, and 1.79×10^{-2} min^{-1} for TO, TO-0.1F, 0.4F, and 1.6F, respectively. The optimal k for TO-0.4F is about 1.67 times that of pristine TO, demonstrating that surface modification by F^- is beneficial to enhance the photocatalytic activity of TiO_2. In addition, the colorless phenol was also used as a model pollutant to evaluate the photocatalytic activity of the as-prepared TO and TO-*x*F samples, as shown in Figure S5. Similarly, the TO-0.4F catalyst exhibits an excellent and higher photocatalytic degradation rate of phenol, compared with that of pristine TO, TO-0.1F, and TO-1.6F.

https://doi.org/10.1021/acsomega.1c05891
ACS Omega 2021, 6, 35799−35809

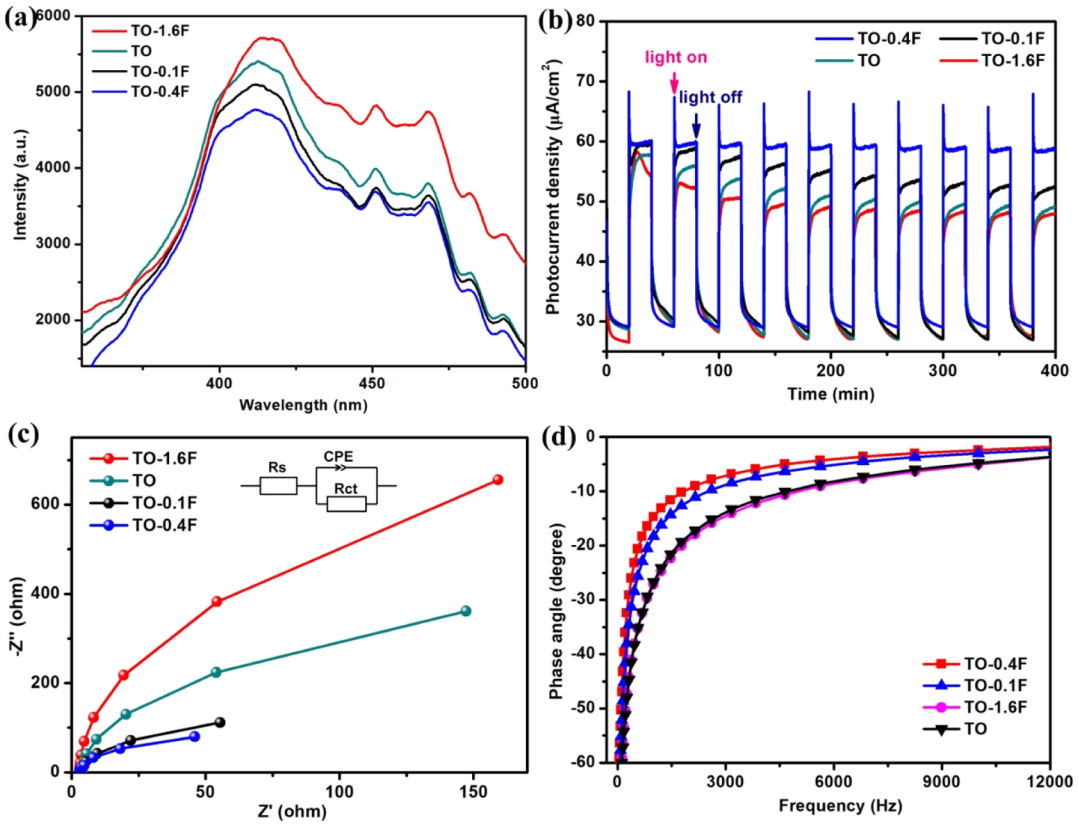

Figure 7. (a) Steady PL spectra; (b) *i*–*t* curves; (c) EIS Nyquist plots; and (d) Bode plot of as-prepared TO-*x*F.

The photocatalytic redox activities were further investigated by the production of hydroxyl radicals (•OH) under UV light irradiation. The relative concentration of •OH is determined by examining the PL intensity centered at 426 nm, as shown in Figure 6c. TO-0.4F and TO-0.1F exhibit higher •OH generation than pure TO, and TO-0.4F shows the highest •OH production performance among the series samples, as shown in Figure 6d. The above results demonstrate that the photoinduced oxidation activity is enhanced in TO-*x*F as compared with pure TO. The photocatalytic degradation reactions generally proceed either directly through photogenerated holes or indirectly through oxidation mediated by the •OH radical. Due to the much higher redox potential of the $F^{\bullet}/F^{-}$ couple (3.6 V), the holes in the VB cannot oxidize the fluorine groups on the TiO_2 surface. Therefore, more •OH radicals are generated in the TO-*x*F catalyst to participate in the photocatalytic reactions. Thus, the hole-induced oxidation of water-producing •OH radicals is highly favored. When the surface of TiO_2 is hydroxylated, the reaction precedes either through the surface trapping of holes or direct electron transfer. In contrast, when the surface is covered by F^-, the kinetic path of the reaction is dominated by the sub-surface holes and free •OH.[48] Therefore, most of the reaction proceeds on the fluorinated TiO_2 through the free •OH radical pathway. However, a too high concentration of surface F^- becomes a new recombination center for photogenerated charge carriers, which leads to lower photocatalytic activity and production rates of •OH radicals. To examine the stability features, three cycles of degradation of MO were tested for TO and TO-0.4F, as shown in Figure S6. It can be seen that the MO degradation efficiency over TO-0.4F after cycling three times is still retained about 95%, which is much higher than that of pristine TO (ca. 80%).

In order to trace the origin of the enhanced photocatalytic activity over TO-*x*F, the PL spectra of TO and TO-*x*F was first examined to evaluate the charge separation behavior. Figure 7a shows the PL spectra of pristine TO and TO-*x*F catalysts. It is worth noting that the TO and TO-*x*F samples exhibit a strong and wide PL signal in the range from 350 to 550 nm, having two obvious PL peaks at about 420 and 480 nm, which are attributed to band-edge-free excitons and bound excitons, respectively.[61] These PL signals are generally attributed to excitonic PL signals, which mainly result from surface oxygen vacancies and defects of TiO_2 nanoparticles.[62] In addition, it can be found that an appropriate amount of surface F^- modification (such as TO-0.1F and TO-0.4F) can efficiently promote the separation of photogenerated carriers and thus reduce the excitonic PL signals. However, too high a surface fluoride ion will form more surface defect sites, which acts as new recombination centers of carriers and leads to enhanced excitonic PL signals (such as TO-1.6F). The above discussions demonstrate that the weaker the excitonic PL spectrum, the higher the separation rate of photoinduced electrons and holes, during the F^- surface-modification of TiO_2. The optimal F^- on the TO surface can boost the transport and separation of carriers, thereby improving its photocatalytic performance. To further ascertain the key role of F^- toward the separation of photoinduced charge carriers, the transient photocurrent response was established under UV light irradiation. As depicted in Figure 7b, the transient photocurrent densities of TO-0.1F and TO-0.4F increase up to 55 and 69 $\mu A\ cm^{-2}$, which are 1.1 and 1.4 times that of pristine TO (48 $\mu A\ cm^{-2}$), respectively. These excellent photocurrents further verify that

https://doi.org/10.1021/acsomega.1c05891
ACS Omega 2021, 6, 35799−35809

F^- surface modification of TiO_2 can remarkably boost the separation of photogenerated charge carriers. However, compared with that of TO, the TO-1.6F sample exhibits a decreased photocurrent density of only 47 μA cm^{-2}, which is consistent with the PL results. In addition, EIS measurements were further conducted to examine the charge-transfer process of as-prepared TO and TO-*x*F samples. As depicted in Figure 7c, the arc radius of TO-0.4F, which is attributed to the whole charge-transfer resistance (R_{ct}), is the smallest, further confirming that the optimal amount of F^- is favorable to promote the transfer of photoinduced charge carriers. The fitted values of R_{ct} (Table S3) for TO, TO-0.1F, TO-0.4F, and TO-1.6F are 913.1, 294.9, 289.9, and 1053 Ω, respectively. This conclusion can be further validated by the Mott−Schottky measurement, as shown in Figure S7. More importantly, the calculated flat band potentials (vs NHE) are in the order of TO (−0.12 V) < TO-0.1F (−0.10 V) = TO-1.6F (−0.10 V) < TO-0.4F (−0.08 V). Further analysis shows that a positive shift in flat band potentials of TO-*x*F compared with that of the TO catalyst can be found, which indicates the decrease in the bending of the band edge and acceleration of the separation and transportation of photogenerated carriers. Moreover, the Mott−Schottky plots for TO and TO-*x*F depict a positive slope, indicating that they are all n-type semiconductors. Based on the slope of Mott−Schottky curves, the calculated carrier density of TO-0.4F is 14.65 × 10^{19} cm^{-3}, which is remarkably higher than that of pure TO (11.71 × 10^{19} cm^{-3}), as shown in Figure S8. The higher carrier density implies that the carrier separation and transport for TO-0.4F is faster than that of pure TO. Moreover, the Bode plot (Figure 7d) is used to reveal the charge-transfer behaviors over bare TO and TO-*x*F catalysts. Compared with bare TO, the frequency peak of TO-0.4F shifts to a lower frequency position, revealing a faster electron transport process. According to the correlation between the frequency (f) and the lifetime of injected electrons: $\tau_e = 1/(2\pi f)$,[63,64] the calculated τ_e for TO-0.4F is 114.6 μs, which is much longer than those of pure TO (75.6 μs),TO-0.1F(98.5 μs), and TO-1.6F(71.1 μs). Based on the above analysis, we confirm that the presence of an optimal amount of F^- on the surface could facilitate the charge separation and transfer of TiO_2, which is indispensable to enhancing its photocatalytic activities. Moreover, due to the strong electronegativity, F^- could serve as a surface trapping site to extract the photogenerated holes from the bulk to the surface of TiO_2, which facilitates the separation of charge carriers and increase the possibilities of the photocatalytic reaction. However, too much F^- could serve as a new recombination center for photogenerated charge carriers and lead to a decreased lifetime of the photogenerated electrons.

U_{OC} was measured to investigate the surface charge trapping of TO and TO-*x*F catalysts, as shown in Figure 8. When one electrode is immersed in the electrolyte, the increase of photoinduced U_{OC} largely depended on the photoinduced charge carrier density, thereby generating a new quasi-Fermi level. Generally, the photovoltage difference under light and dark conditions can directly reflect the potential loss of reaction kinetics in the Helmholtz layer on the surface of the catalyst.[65] The photovoltage for TO-0.4F is detected to be 0.29 V, which is 0.25 V higher than that of pure TO. The increased U_{OC} over TO-0.4F implies that F^- surface modification can boost surface charge trapping, thereby leading to both the higher separation efficiency and transfer efficiency of charge carriers.

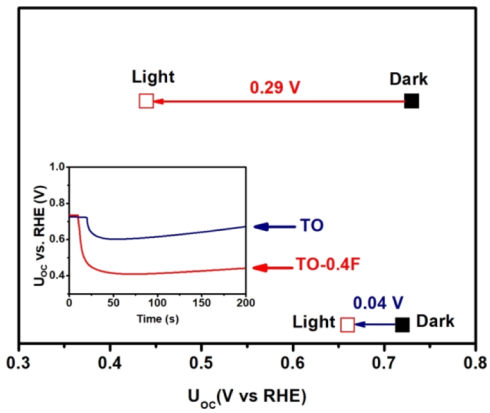

Figure 8. Open circuit potentials (U_{OC}) of TO and TO-*x*F tested under dark (solid, black) and illumination (hollow, red); inset: transient photovoltage response to immediate illumination.

The PL decay curves shown in Figure 9 could provide information about the recombination of free charges located near the edge of the band, rather than the recombination caused by deep trapped charges.[66,67] Compared with pristine TO, all the TO-xF samples give two radiative lifetimes over the deconvolution of the fluorescence decay spectra, as listed in Table S3. As for TO-0.1F, TO-0.4F, and TO-1.6F catalysts, the population of the short-lived charge carriers (1.02, 1.08, and 0.98 ns for TO-0.1F, TO-0.4F, and TO-1.6F) is greatly reduced (31.2, 32.2, and 25.2% for TO-0.1F, TO-0.4F, and TO-1.6F, respectively) compared with that of pure TO (100%), which results from the rapid recombination of photoinduced electrons and holes. However, compared with pure TO, the percentage of charge carriers with a lifetime longer than 2.5 ns for TO-0.1F and TO-0.4F tremendously increases, respectively, to 68.8 and 67.8%, which is beneficial to increase the possibility of charge carriers to participate in the photocatalytic reaction. The change in the percentage of short/long-lived charge carriers might be related to the localized defective sites associated with F^- in the energy band of TiO_2. In addition, the high concentration of long-lived trapped electrons and holes increases the probability of contact with the reactants, thereby improving the photocatalytic activity of TiO_2. In addition, the calculated average carrier lifetime(τ)

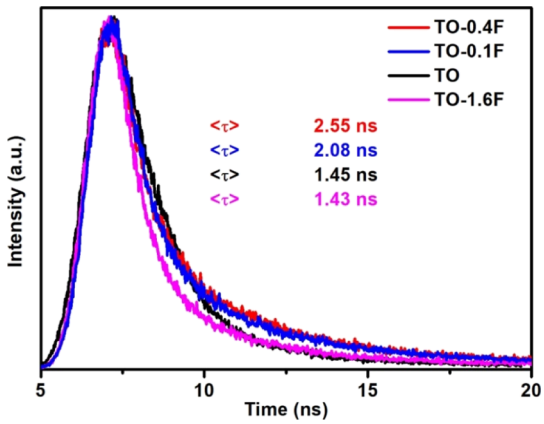

Figure 9. Time-resolved PL decay spectra over TO and TO-*x*F.

https://doi.org/10.1021/acsomega.1c05891
ACS Omega 2021, 6, 35799−35809

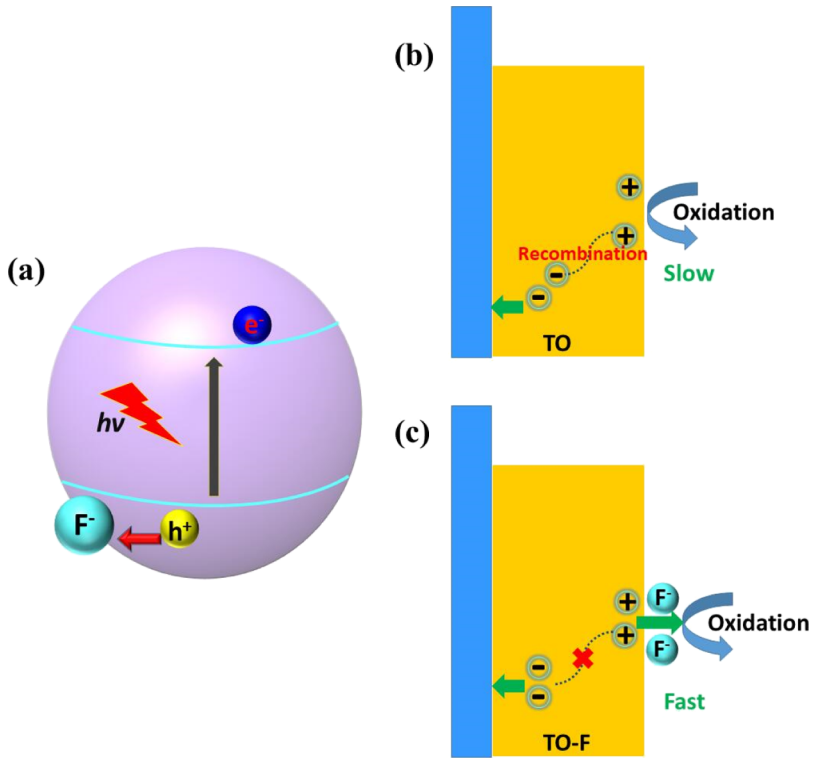

Figure 10. (a) Proposed mechanism for F^--promoted surface charge separation of TO-F. Schematic diagram of F^--modified TO-promoted carrier charge separation and accelerated photoelectrochemical performance for (b) TO and (c) TO-F photoanodes.

order is as follows: TO-0.4F (2.55 ns) > TO-0.1F (2.08 ns) > TO-0.4F (1.45 ns) > TO-0.4F (1.43 ns).

To compare the energy band structure differences between pristine TO and TO-*x*F, the energy levels of both conduction band (CB) and valence band (VB) potentials are provided, as shown in Figure S9. According to the formula $E_g = E_v - E_c$ (E_g: band gap, E_v: VB potential, and E_c: CB potential), the CB potentials of TO and TO-0.4F were calculated to be −0.49 and 0.35 eV, respectively. Moreover, it can be found that the VB potential of TO-0.4F downward shifts to 2.59 eV compared with that of pure TO (VB maximum at 2.42 eV). The downward shift of the VB implies that the oxidizing ability of the photogenerated holes in TO-0.4F may become stronger, which is beneficial to the photocatalytic oxidation reactions. Based on the above-mentioned characterization analysis and band structure, a possible photocatalytic mechanism over the TO-*x*F catalyst is proposed, which is illustrated in Figure 10. As can be seen from Figure 10a, by coupling F^- species with the strong electronegativity on the surface of TO, the photogenerated holes could be trapped, and the migration and separation of photogenerated electrons to reactive sites to participate in the redox reactions are highly promoted. As for the photoelectrochemical reaction, it is reasonably inferred that F^- on the surface of TO inhibits the recombination rates of charge carriers and facilitates electron−hole pairs of separation and hole transfer, which finally leads to the enhancement of the photoelectrochemical performance. The F^--enhanced surface trapping sites and hole transfer through the solid/liquid interface is shown in Figure 10b,c.

4. CONCLUSIONS

In summary, a series of surface F^--modified TiO_2 (P25) catalysts were prepared by a facile post-treatment at room temperature. The effects of F^- toward the geometrical morphology, chemical state, optical absorption, surface electronic structure, and energy band alignment of TiO_2 are systematically analyzed. Compared with pure TO, the TO-0.4F sample exhibits enhanced photocatalytic degradation of MO and phenol, production of OH radicals, and photocurrent response irradiated under ultraviolet light. The improved photocatalytic performance of TO-0.4F can be attributed to the fact that F^- acts as surface trapping sites to promote the transfer and separation of photogenerated charge carriers, which is validated by steady PL spectra, EIS plot, Bode plot, open circuit potential measurement, and time-resolved PL decay spectra. This work highlights the role of surface F^- modification in boosting the separation and transfer of charge carriers and ultimately enhancing the photocatalytic activity of TiO_2.

■ ASSOCIATED CONTENT

Supporting Information

The Supporting Information is available free of charge at https://pubs.acs.org/doi/10.1021/acsomega.1c05891.

SEM images of TO and TO-*x*F; EDX patterns of TO-0.4F; FTIR spectra; N_2 adsorption/desorption isotherms; photocatalytic degradation of phenol over TO and TO-*x*F catalysts; schematic of the atomic surface structure of anatase TiO_2; stability test of degradation of MO over TO and TO-0.4F catalysts; Mott−Schottky plots; carrier density of TO and TO-*x*F; and schematic diagram representing the electronic structure of as-prepared TO and TO-0.4F catalysts (PDF)

https://doi.org/10.1021/acsomega.1c05891
ACS Omega 2021, 6, 35799−35809

AUTHOR INFORMATION

Corresponding Author

Xiaogang Liu − *College of Chemistry and Chemical Engineering and Henan Province Key Laboratory of Utilization of Non Metallic Mineral in the South of Henan, Xinyang Normal University, Xinyang, Henan 464000, P. R. China;* orcid.org/0000-0002-2063-1956; Email: lxg133298@163.com

Authors

Wenjie Chen − *College of Chemistry and Chemical Engineering, Xinyang Normal University, Xinyang, Henan 464000, P. R. China*

Wei Wang − *State Key Laboratory of High-efficiency Utilization of Coal and Green Chemical Engineering, Ningxia University, Yinchuan 750021, P. R.China*

Complete contact information is available at: https://pubs.acs.org/10.1021/acsomega.1c05891

Notes

The authors declare no competing financial interest.

ACKNOWLEDGMENTS

This study was supported by the National Natural Science Foundation of China (21902140), Foundation of State Key Laboratory of High-efficiency Utilization of Coal and Green Chemical Engineering (grant no. 2021-K47), and the Nanhu Scholars Program for Young Scholars of XYNU.

REFERENCES

(1) Gallo, A.; Montini, T.; Marelli, M.; Minguzzi, A.; Gombac, V.; Psaro, R.; Fornasiero, P.; Dal Santo, V. H_2 Production by Renewables Photoreforming on Pt-Au/TiO_2 Catalysts Activated by Reduction. *Chemsuschem* **2012**, *5*, 1800−1811.

(2) Fang, S. Y.; Liu, Y. X.; Sun, Z. X.; Lang, J. Y.; Bao, C. Y.; Hu, Y. H. Photocatalytic hydrogen production over Rh-loaded TiO_2: What is the origin of hydrogen and how to achieve hydrogen production from water? *Appl. Catal., B* **2020**, *278*, 119316.

(3) Chen, X.; Gierlich, C. H.; Schötz, S.; Blaumeiser, D.; Bauer, T.; Libuda, J.; Palkovits, R. Hydrogen Production Based on Liquid Organic Hydrogen Carriers through Sulfur Doped Platinum Catalysts Supported on TiO_2. *ACS Sustainable Chem. Eng.* **2021**, *9*, 6561−6573.

(4) Li, D.; Zhou, C. J.; Xie, Z. K.; Chen, D. H.; Zhou, Y. M.; Shi, X. L.; Jiang, D. L.; Chen, M.; Shi, W. D. Steering Multistep Charge Transfer for Highly Selectively Photocatalytic Reduction of CO_2 into CH_4 over Pd/Cu_2O/TiO_2 Ternary Hybrid. *Sol. RRL* **2021**, *5*, 2000813.

(5) Tang, K.; Wang, Z.; Zou, W.; Guo, H.; Wu, Y.; Pu, Y.; Tong, Q.; Wan, H.; Gu, X.; Dong, L.; Rong, J.; Chen, Y.-W. Advantageous Role of Ir-0 Supported on TiO_2 Nanosheets in Photocatalytic CO_2 Reduction to CH4: Fast Electron Transfer and Rich Surface Hydroxyl Groups. *ACS Appl. Mater. Interfaces* **2021**, *13*, 6219−6228.

(6) Wang, A.; Wu, S. J.; Dong, J. L.; Wang, R. X.; Wang, J. W.; Zhang, J. L.; Zhong, S. X.; Bai, S. Interfacial facet engineering on the Schottky barrier between plasmonic Au and TiO_2 in boosting the photocatalytic CO_2 reduction under ultraviolet and visible light irradiation. *Chem. Eng. J.* **2021**, *404*, 127145.

(7) Wang, Z. W.; Wan, Q.; Shi, Y. Z.; Wang, H.; Kang, Y. Y.; Zhu, S. Y.; Lin, S.; Wu, L. Selective photocatalytic reduction CO_2 to CH_4 on ultrathin TiO_2 nanosheet via coordination activation. *Appl. Catal., B* **2021**, *288*, 120000.

(8) Zhao, Y. X.; Zhao, Y. F.; Shi, R.; Wang, B.; Waterhouse, G. I. N.; Wu, L. Z.; Tung, C. H.; Zhang, T. R. Tuning Oxygen Vacancies in Ultrathin TiO_2 Nanosheets to Boost Photocatalytic Nitrogen Fixation up to 700 nm. *Adv. Mater.* **2019**, *31*, 1806482.

(9) Li, C.; Wang, T.; Zhao, Z.-J.; Yang, W.; Li, J.-F.; Li, A.; Yang, Z.; Ozin, G. A.; Gong, J. Promoted Fixation of Molecular Nitrogen with Surface Oxygen Vacancies on Plasmon-Enhanced TiO_2 Photoelectrodes. *Angew. Chem., Int. Ed.* **2018**, *57*, 5278−5282.

(10) Zhang, G.; Yang, X.; He, C.; Zhang, P.; Mi, H. Constructing a tunable defect structure in TiO_2 for photocatalytic nitrogen fixation. *J. Mater. Chem. A* **2020**, *8*, 334−341.

(11) Hoffmann, M. R.; Martin, S. T.; Choi, W.; Bahnemann, D. W. Environmental Applications Of Semiconductor Photocatalysis. *Chem. Rev.* **1995**, *95*, 69−96.

(12) Mehmood, C. T.; Zhong, Z. Y.; Zhou, H.; Xiao, Y. Y. Constructing porous beads with modified polysulfone-alginate and TiO_2 as a robust and recyclable photocatalyst for wastewater treatment. *J. Water Proc. Eng.* **2020**, *38*, 101601.

(13) Pandiyaraj, K. N.; Vasu, D.; Ghobeira, R.; Tabaei, P. S. E.; De Geyter, N.; Morent, R.; Pichumani, M.; Padmanabhanan, P. V. A.; Deshmukh, R. R. Dye wastewater degradation by the synergetic effect of an atmospheric pressure plasma treatment and the photocatalytic activity of plasma-functionalized Cu-TiO_2 nanoparticles. *J. Hazard. Mater.* **2021**, *405*, 124264.

(14) Chang, T. J.; Hsueh, T. J. A NO_2 Gas Sensor with a TiO_2 Nanoparticles/ZnO/MEMS-Structure that is Produced Using Ultrasonic Wave Grinding Technology. *J. Electrochem. Soc.* **2020**, *167*, 027521.

(15) Harathi, N.; Sarkar, A. TiO_2 based surface acoustic wave gas sensor with modified electrode dimensions for enhanced H_2 sensing application. *Int. J. Nano Dimens.* **2021**, *12*, 83−89.

(16) Singh, T.; Oz, S.; Sasinska, A.; Frohnhoven, R.; Mathur, S.; Miyasaka, T. Sulfate-Assisted Interfacial Engineering for High Yield and Efficiency of Triple Cation Perovskite Solar Cells with Alkali-Doped TiO_2 Electron-Transporting Layers. *Adv. Funct. Mater.* **2018**, *28*, 1706287.

(17) Tavakoli, M. M.; Yadav, P.; Tavakoli, R.; Kong, J. Surface Engineering of TiO_2 ETL for Highly Efficient and Hysteresis-Less Planar Perovskite Solar Cell (21.4%) with Enhanced Open-Circuit Voltage and Stability. *Adv. Energy Mater.* **2018**, *8*, 1800794.

(18) Zhang, Y.; Zhang, P.; Zhang, S.; Wang, Z.; Li, N.; Silva, S. R. P.; Shao, G. A flexible metallic TiC nanofiber/vertical graphene 1D/2D heterostructured as active electrocatalyst for advanced Li-S batteries. *InfoMat* **2021**, *3*, 790−803.

(19) Zhang, S.; Zhang, P.; Hou, R.; Li, B.; Zhang, Y.; Liu, K.; Zhang, X.; Shao, G. In situ sulfur-doped graphene nanofiber network as efficient metal-free electrocatalyst for polysulfides redox reactions in lithium−sulfur batteries. *J. Energy Chem.* **2020**, *47*, 281−290.

(20) Zhang, P.; Li, Y.; Zhang, Y.; Hou, R.; Zhang, X.; Xue, C.; Wang, S.; Zhu, B.; Li, N.; Shao, G. Photogenerated Electron Transfer Process in Heterojunctions: In Situ Irradiation XPS. *Small Methods* **2020**, *4*, 2000214.

(21) Li, D.; Chen, S.; You, R.; Liu, Y.; Yang, M.; Cao, T.; Qian, K.; Zhang, Z.; Tian, J.; Huang, W. Titania-morphology-dependent dual-perimeter-sites catalysis by Au/TiO_2 catalysts in low-temperature CO oxidation. *J. Catal.* **2018**, *368*, 163−171.

(22) Chen, S.; Abdel-Mageed, A. M.; Li, D.; Bansmann, J.; Cisneros, S.; Biskupek, J.; Huang, W.; Behm, R. J. Morphology-Engineered Highly Active and Stable Ru/TiO_2 Catalysts for Selective CO Methanation. *Angew. Chem., Int. Ed.* **2019**, *58*, 10732−10736.

(23) Zong, L.; Zhang, G.; Zhao, J.; Dong, F.; Zhang, J.; Tang, Z. Morphology-controlled synthesis of 3D flower-like TiO_2 and the superior performance for selective catalytic reduction of NO_x with NH_3. *Chem. Eng. J.* **2018**, *343*, 500−511.

(24) Yang, H. G.; Sun, C. H.; Qiao, S. Z.; Zou, J.; Liu, G.; Smith, S. C.; Cheng, H. M.; Lu, G. Q. Anatase TiO_2 single crystals with a large percentage of reactive facets. *Nature* **2008**, *453*, 638−641.

(25) Liu, G.; Yang, H. G.; Pan, J.; Yang, Y. Q.; Lu, G. Q.; Cheng, H.-M. Titanium dioxide crystals with tailored facets. *Chem. Rev.* **2014**, *114*, 9559−9612.

(26) Zhang, H.; Cai, J.; Wang, Y.; Wu, M.; Meng, M.; Tian, Y.; Li, X.; Zhang, J.; Zheng, L.; Jiang, Z.; Gong, J. Insights into the effects of

surface/bulk defects on photocatalytic hydrogen evolution over TiO_2 with exposed {001} facets. *Appl. Catal., B* **2018**, *220*, 126−136.
(27) Yu, J. C.; Yu, J. G.; Ho, W. K.; Jiang, Z. T.; Zhang, L. Z. Effects of F- doping on the photocatalytic activity and microstructures of nanocrystalline TiO_2 powders. *Chem. Mater.* **2002**, *14*, 3808−3816.
(28) Park, J. H.; Kim, S.; Bard, A. J. Novel carbon-doped TiO_2 nanotube arrays with high aspect ratios for efficient solar water splitting. *Nano Lett.* **2006**, *6*, 24−28.
(29) Burda, C.; Lou, Y.; Chen, X.; Samia, A. C. S.; Stout, J.; Gole, J. L. Enhanced nitrogen doping in TiO_2 nanoparticles. *Nano Lett.* **2003**, *3*, 1049−1051.
(30) Qin, Y.; Li, H.; Lu, J.; Meng, F.; Ma, C.; Yan, Y.; Meng, M. Nitrogen-doped hydrogenated TiO_2 modified with CdS nanorods with enhanced optical absorption, charge separation and photocatalytic hydrogen evolution. *Chem. Eng. J.* **2020**, *384*, 123275.
(31) Gong, S.; Fan, J.; Cecen, V.; Huang, C.; Min, Y.; Xu, Q.; Li, H. Noble-metal and cocatalyst free W_2N/C/TiO photocatalysts for efficient photocatalytic overall water splitting in visible and near-infrared light regions. *Chem. Eng. J.* **2021**, *405*, 126913.
(32) Hao, J.; He, H.; Gong, S.; Fan, J.; Xu, Q.; Min, Y. WN Coupled with Bi Nanoparticles to Enhance the Localized Surface Plasmon Resonance Effect for Photocatalytic Hydrogen Evolution. *ACS Appl. Mater. Interfaces* **2021**, *13*, 19884−19893.
(33) Hao, J.; Yang, D.; Wu, J.; Ni, B.; Wei, L.; Xu, Q.; Min, Y.; Li, H. Utilizing new metal phase nanocomposites deep photocatalytic conversion of CO_2 to C_2H_4. *Chem. Eng. J.* **2021**, *423*, 130190.
(34) Li, Y.; Zhang, P.; Wan, D.; Xue, C.; Zhao, J.; Shao, G. Direct evidence of 2D/1D heterojunction enhancement on photocatalytic activity through assembling MoS_2 nanosheets onto super-long TiO_2 nanofibers. *Appl. Surf. Sci.* **2020**, *504*, 144361.
(35) Liu, Y.; Li, Y.; Peng, F.; Lin, Y.; Yang, S.; Zhang, S.; Wang, H.; Cao, Y.; Yu, H. 2H-and 1T-mixed phase few-layer MoS_2 as a superior to Pt co-catalyst coated on TiO_2 nanorod arrays for photocatalytic hydrogen evolution. *Appl. Catal., B* **2019**, *241*, 236−245.
(36) Tanaka, A.; Teramura, K.; Hosokawa, S.; Kominami, H.; Tanaka, T. Visible light-induced water splitting in an aqueous suspension of a plasmonic Au/TiO_2 photocatalyst with metal co-catalysts. *Chem. Sci.* **2017**, *8*, 2574−2580.
(37) Zhang, G.; Sun, Y.; Zhang, C.; Yu, Z. Decomposition of acetaminophen in water by a gas phase dielectric barrier discharge plasma combined with TiO_2-rGO nanocomposite: Mechanism and degradation pathway. *J. Hazard. Mater.* **2017**, *323*, 719−729.
(38) He, H. N.; Huang, D.; Pang, W. K.; Sun, D.; Wang, Q.; Tang, Y. G.; Ji, X. B.; Guo, Z. P.; Wang, H. Y. Plasma-Induced Amorphous Shell and Deep Cation-Site S Doping Endow TiO_2 with Extraordinary Sodium Storage Performance. *Adv. Mater.* **2018**, *30*, 1801013.
(39) Zhang, Y.; Zhang, P.; Li, B.; Zhang, S.; Liu, K.; Hou, R.; Zhang, X.; Silva, S. R. P.; Shao, G. Vertically aligned graphene nanosheets on multi-yolk/shell structured TiC@C nanofibers for stable Li-S batteries. *Energy Storage Mater.* **2020**, *27*, 159−168.
(40) Zhang, Q.; Liu, M.; Zhou, W.; Zhang, Y.; Hao, W.; Kuang, Y.; Liu, H.; Wang, D.; Liu, L.; Ye, J. A novel Cl- modification approach to develop highly efficient photocatalytic oxygen evolution over $BiVO_4$ with AQE of 34.6. *Nano Energy* **2021**, *81*, 105651.
(41) Li, Z.; Zhang, Q.; Chen, X.; Yang, F.; Wang, D.; Liu, L.; Ye, J. Cl modification for effective promotion of photoelectrochemical water oxidation over $BiVO_4$. *Chem. Commun.* **2020**, *56*, 13153.
(42) Li, Y.-Y.; Fan, J.-S.; Tan, R.-Q.; Yao, H.-C.; Peng, Y.; Liu, Q.-C.; Li, Z.-J. Selective Photocatalytic Reduction of CO_2 to CH_4 Modulated by Chloride Modification on Bi2WO6 Nanosheets. *ACS Appl. Mater. Interfaces* **2020**, *12*, 54507−54516.
(43) Liu, X.; Dong, G.; Li, S.; Lu, G.; Bi, Y. Direct Observation of Charge Separation on Anatase TiO_2 Crystals with Selectively Etched {001} Facets. *J. Am. Chem. Soc.* **2016**, *138*, 2917−2920.
(44) Li, Y.; Yin, Z.; Ji, G.; Liang, Z.; Xue, Y.; Guo, Y.; Tian, J.; Wang, X.; Cui, H. 2D/2D/2D heterojunction of Ti_3C_2 MXene/MoS_2 nanosheets/TiO_2 nanosheets with exposed (001) facets toward enhanced photocatalytic hydrogen production activity. *Appl. Catal., B* **2019**, *246*, 12−20.
(45) Khan, J. A.; Sayed, M.; Shah, N. S.; Khan, S.; Zhang, Y. X.; Boczkaj, G.; Khan, H. M.; Dionysiou, D. D. Synthesis of eosin modified TiO_2 film with co-exposed {001} and {101} facets for photocatalytic degradation of para-aminobenzoic acid and solar H_2 production. *Appl. Catal., B* **2020**, *265*, 118557.
(46) Zha, C.; Gu, X.; Wu, D.; Chen, H. Interfacial active fluorine site-induced electron transfer on TiO_2 (001) facets to enhance polysulfide redox reactions for better liquid Li_2S_6-Based lithium-sulfur batteries. *J. Mater. Chem. A* **2019**, *7*, 6431−6438.
(47) Fessi, N.; Nsib, M. F.; Cardenas, L.; Guillard, C.; Dappozze, F.; Houas, A.; Parrino, F.; Palmisano, L.; Ledoux, G.; Amans, D.; Chevalier, Y. Surface and Electronic Features of Fluorinated TiO_2 and Their Influence on the Photocatalytic Degradation of 1-Methylnaphthalene. *J. Phys. Chem. C* **2020**, *124*, 11456−11468.
(48) Minero, C.; Mariella, G.; Maurino, V.; Pelizzetti, E. Photocatalytic Transformation of Organic Compounds in the Presence of Inorganic Anions. 1. Hydroxyl-Mediated and Direct Electron-Transfer Reactions of Phenol on a Titanium DioxideFluoride System. *Langmuir* **2000**, *16*, 2632−2641.
(49) Park, H.; Choi, W. Effects of TiO_2 surface fluorination on photocatalytic reactions and photoelectrochemical behaviors. *J. Phys. Chem. B* **2004**, *108*, 4086−4093.
(50) Park, J. S.; Choi, W. Enhanced remote photocatalytic oxidation on surface-fluorinated TiO_2. *Langmuir* **2004**, *20*, 11523−11527.
(51) Vohra, M. S.; Kim, S.; Choi, W. Effects of surface fluorination of TiO_2 on the photocatalytic degradation of tetramethylammonium. *J. Photochem. Photobiol., A* **2003**, *160*, 55−60.
(52) Zhang, P.; Li, Y. K.; Zhang, Y. S.; Hou, R. H.; Zhang, X. L.; Xue, C.; Wang, S. B.; Zhu, B. C.; Li, N.; Shao, G. S. Photogenerated Electron Transfer Process in Heterojunctions: In Situ Irradiation XPS. *Small Methods* **2020**, *4*, 2000214.
(53) Minero, C.; Mariella, G.; Maurino, V.; Vione, D.; Pelizzetti, E. Photocatalytic Transformation of Organic Compounds in the Presence of Inorganic Ions. 2. Competitive Reactions of Phenol and Alcohols on a Titanium Dioxide-Fluoride System. *Langmuir* **2000**, *16*, 8964−8972.
(54) Jańczyk, A.; Krakowska, E.; Stochel, G. Singlet Oxygen Photogeneration at Surface Modified Titanium Dioxide. *J. Am. Chem. Soc.* **2006**, *128*, 15574−15575.
(55) Dozzi, M.; Selli, E. Specific Facets-Dominated Anatase TiO_2: Fluorine-Mediated Synthesis and Photoactivity. *Catalysts* **2013**, *3*, 455−485.
(56) Yang, Y.; Ye, K.; Cao, D.; Gao, P.; Qiu, M.; Liu, L.; Yang, P. Efficient Charge Separation from F^- Selective Etching and Doping of Anatase-TiO_2{001} for Enhanced Photocatalytic Hydrogen Production. *ACS Appl. Mater. Interfaces* **2018**, *10*, 19633−19638.
(57) Eleutério, T.; Sério, S.; Teodoro, O. M. N. D.; Bundaleski, N.; Vasconcelos, H. C. XPS and FTIR Studies of DC Reactive Magnetron Sputtered TiO_2 Thin Films on Natural Based-Cellulose Fibers. *Coatings* **2020**, *10*, 287.
(58) Bezrodna, T.; Puchkovska, G.; Shymanovska, V.; Baran, J.; Ratajczak, H. IR-analysis of H-bonded H_2O on the pure TiO_2 surface. *J. Mol. Struct.* **2004**, *700*, 175−181.
(59) Ba-Abbad, M. M.; Kadhum, A. A. H.; Mohamad, A. B.; Takriff, M. S.; Sopian, K. Synthesis and Catalytic Activity of TiO_2 Nanoparticles for Photochemical Oxidation of Concentrated Chlorophenols under Direct Solar Radiation. *Int. J. Electrochem. Sci.* **2012**, *7*, 4871−4888.
(60) Švagelj, Z.; Mandic, V.; Curkovic, L.; Biosic, M.; Zmak, I.; Gaborardi, M. Titania-Coated Alumina Foam Photocatalyst for Memantine Degradation Derived by Replica Method and Sol-Gel Reaction. *Materials* **2020**, *13*, 227.
(61) Liqiang, J.; Yichun, Q.; Baiqi, W.; Shudan, L.; Baojiang, J.; Libin, Y.; Wei, F.; Honggang, F.; Jiazhong, S. Review of photoluminescence performance of nano-sized semiconductor materials and its relationships with photocatalytic activity. *Sol. Energy Mater. Sol. Cells* **2006**, *90*, 1773−1787.
(62) Liqiang, J.; Xiaojun, S.; Weimin, C.; Zili, X.; Yaoguo, D.; Honggang, F. The preparation and characterization of nanoparticle

https://doi.org/10.1021/acsomega.1c05891
ACS Omega 2021, 6, 35799−35809

TiO_2/Ti films and their photocatalytic activity. *J. Phys. Chem. Solids* **2003**, *64*, 615−623.
(63) Sultana, S.; Mansingh, S.; Parida, K. M. Rational design of light induced self healed Fe based oxygen vacancy rich CeO_2 (CeO_2NS-FeOOH/Fe_2O_3) nanostructure materials for photocatalytic water oxidation and Cr(vi) reduction. *J. Mater. Chem. A* **2018**, *6*, 11377−11389.
(64) Baral, B.; Reddy, K. H.; Parida, K. M. Construction of M-$BiVO_4$/T-$BiVO_4$ isotype heterojunction for enhanced photocatalytic degradation of Norfloxacine and Oxygen evolution reaction. *J. Colloid Interface Sci.* **2019**, *554*, 278−295.
(65) Du, C.; Yang, X.; Mayer, M. T.; Hoyt, H.; Xie, J.; McMahon, G.; Bischoping, G.; Wang, D. Hematite-Based Water Splitting with Low Turn-On Voltages. *Angew. Chem., Int. Ed.* **2013**, *52*, 12692−12695.
(66) Srimath Kandada, A. R.; Neutzner, S.; D'Innocenzo, V.; Tassone, F.; Gandini, M.; Akkerman, Q. A.; Prato, M.; Manna, L.; Petrozza, A.; Lanzani, G. Nonlinear Carrier Interactions in Lead Halide Perovskites and the Role of Defects. *J. Am. Chem. Soc.* **2016**, *138*, 13604−13611.
(67) Merschjann, C.; Tyborski, T.; Orthmann, S.; Yang, F.; Schwarzburg, K.; Lublow, M.; Lux-Steiner, M.-C.; Schedel-Niedrig, T. Photophysics of polymeric carbon nitride: An optical quasimonomer. *Phys. Rev. B: Condens. Matter Mater. Phys.* **2013**, *87*, 205204.

https://doi.org/10.1021/acsomega.1c05891
ACS Omega 2021, 6, 35799−35809